Supporting Information

Universal mechanism of water-sulfur synergistic poisoning on transition metal-doped TiO_2 catalysts for NH_3-SCR

Chaolong Wang[a], Huiling Zheng[a,*], Zhikuan Xin[a], Bing Wang[a], Zhong Li[a,*]

[a] *State Key Laboratory of Clean and Efficient Coal Utilization, College of Chemistry and Chemical Engineering, Taiyuan University of Technology, Taiyuan 030024, China*

[*] *Corresponding authors*

E-mail address: zhenghuiling@tyut.edu.cn(H. Zheng), lizhong@tyut.edu.cn(Z. Li)

Computational and Modeling Methods

All DFT calculations were conducted using the Vienna Ab initio Simulation Package (VASP)[1,2]. The exchange-correlation interactions were described using the generalized gradient approximation with the Perdew-Burke-Ernzerhof functional (GGA-PBE)[3]. Core electrons were described using the projector augmented-wave (PAW) method[4], with valence electrons modeled by a plane-wave basis set with an energy cutoff of 400 eV[5].

The anatase (101) facet was selected as the model surface for this study. This facet is the thermodynamically stable and dominant exposed facet in conventionally synthesized materials[6-9]. Although the highly reactive (001) facet has been explored in specially tailored materials[10,11], the (101) facet remains the most representative for practical catalysts. Based on this, a periodic six-layer slab of anatase TiO_2(101) was constructed from a crystal structure sourced from the Crystallography Open Database (COD)[12]. The slab was built using a (2×2) surface unit cell and included a 15 Å vacuum gap to prevent interactions between periodic images. Doped models (M-TiO_2 (101)) were then constructed by substituting a five-coordinated Ti (Ti_{5c}) site on the surface with a transition metal or Ce atom[13,14], as illustrated in Fig. S1. During structural optimization, the top four layers of atoms were allowed to relax, while the bottom two layers were fixed, with convergence achieved when atomic forces were below 0.05 eV/Å. Brillouin zone integration was performed using a 2×2×1 k-point mesh generated via the Monkhorst-Pack scheme.

To account for the magnetic properties of Mn and other metal ions in M-TiO_2, spin-polarized calculations were conducted for total energy computations. To accurately describe the strong correlation effects of transition metal d-orbitals and Ce f-orbitals, the DFT+U approach with Hubbard corrections was applied, with considering only effective Hubbard parameters (U_{eff}) for each doping metal, as listed in Table S1. Transition states were identified using the climbing-image nudged elastic band (CINEB) method[15], with their validity confirmed by frequency analysis showing a single imaginary frequency along the reaction pathway. Bader charge analysis was conducted to quantify charge transfer and analyze electronic properties[16-19]. Adsorption energies were calculated using the following expression:

$$E_{ads} = E_{all} - E_{slab} - E_x$$

where E_{all} is the total energy of the slab with the adsorbed species, E_{slab} is the energy of the bare slab, and E_x is the energy of the adsorbate in vacuum. A negative E_{ads} indicates an exothermic process, with a larger absolute value signifying stronger adsorption.

Table S1. U_{eff} values for doping transition metals and Ce in M-TiO_2 catalysts

	U_{eff}/eV		U_{eff}/eV		U_{eff}/eV
Sc 3d	5.0[20]	Ni 3d	6.0[23]	Tc 4d	/
Ti 3d	4.2[21]	Cu 3d	6.0[26]	Ru 4d	/
V 3d	3.1[22]	Zn 3d	8.0[27]	Rh 4d	/
Cr 3d	3.5[23]	Y 4d	3.5[28]	Pd 4d	/
Mn 3d	4.5[24]	Zr 4d	4.0[29]	Ag 4d	/
Fe 3d	4.0[25]	Nb 4d	4.0[30]	Cd 4d	2.0[31]
Co 3d	3.4[23]	Mo 4d	3.5[23]	Ce 4f	4.5[32]

Table S2. Bader charge analysis of electron transfer during -NH_4SO_4 formation on Mn-TiO_2 catalyst

System(Mn-TiO_2)	Bader charge change/*e*
$^*H_2O$	-0.12
$^*H_2O$+-SO_4	-0.04
-NH_4SO_4	-0.18

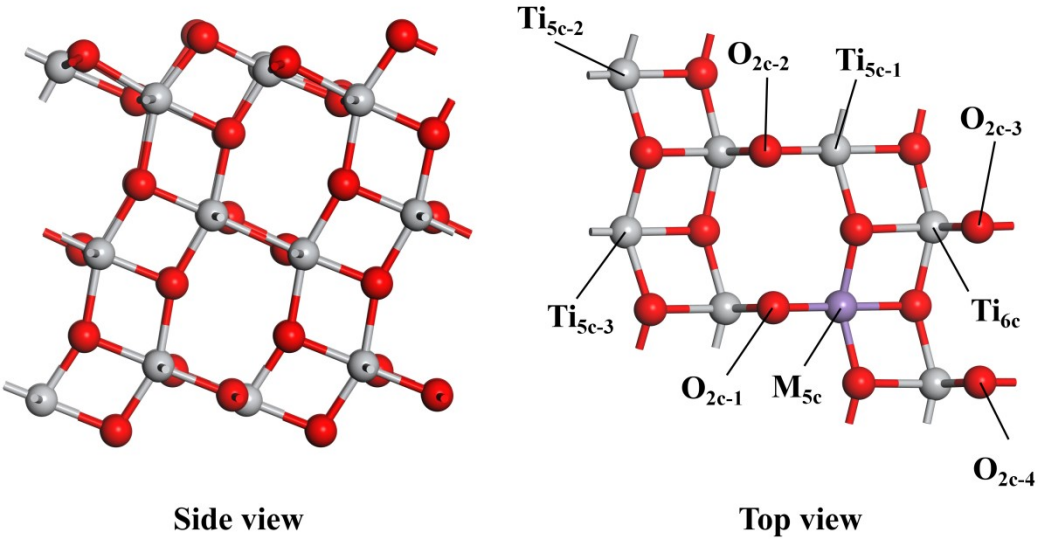

Fig. S1. Structural models of (a) the pristine TiO_2(101) slab and (b) the M-TiO_2(101) catalysts. (Color scheme: gray, Ti; purple, M; red, O. Coordination states: five-coordinated doping metal, M_{5c}; five-coordinated Ti, Ti_{5c}; six-coordinated Ti, Ti_{6c}; two-coordinated O, O_{2c})

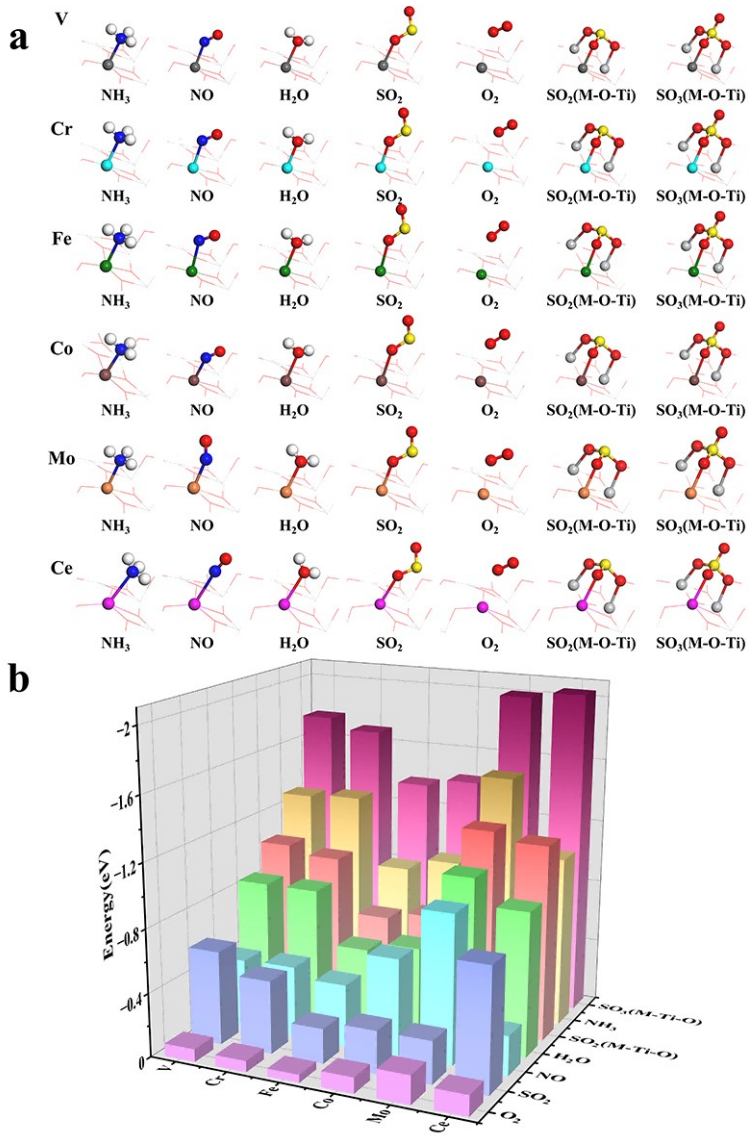

Fig. S2. (a) Adsorption sites and configurations of NH_3 and flue gas molecules (Color scheme: dark grey, V; cyan, Cr; green, Fe; brown, Co; orange, Mo; pink, Ce; grey, Ti; red, O; white, H; blue, N; yellow, S) and (b) their corresponding adsorption energies on M-TiO_2 catalysts (M = V, Cr, Fe, Co, Mo, Ce).

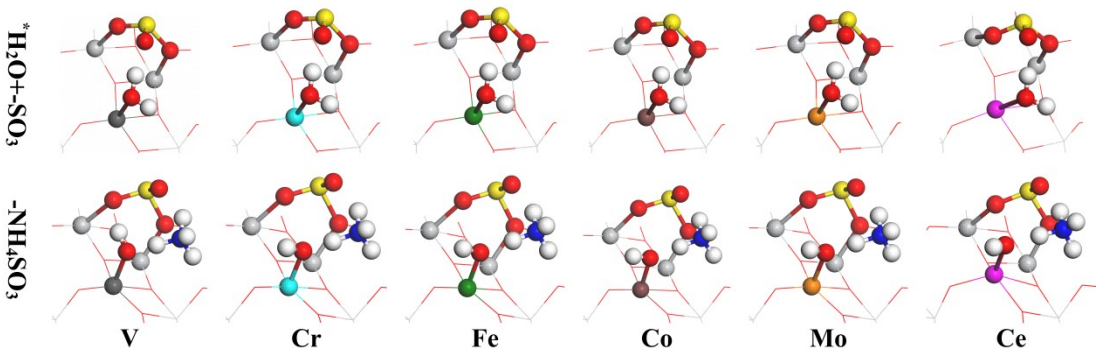

Fig. S3. Configurations of intermediates and products in water-sulfur synergistic poisoning pathways forming -NH_4SO_3 on M-TiO_2 catalysts (M = V, Cr, Fe, Co, Mo, Ce). (Color scheme: dark grey, V; cyan, Cr; green, Fe; brown, Co; orange, Mo; pink, Ce; grey, Ti; red, O; white, H; blue, N; yellow, S)

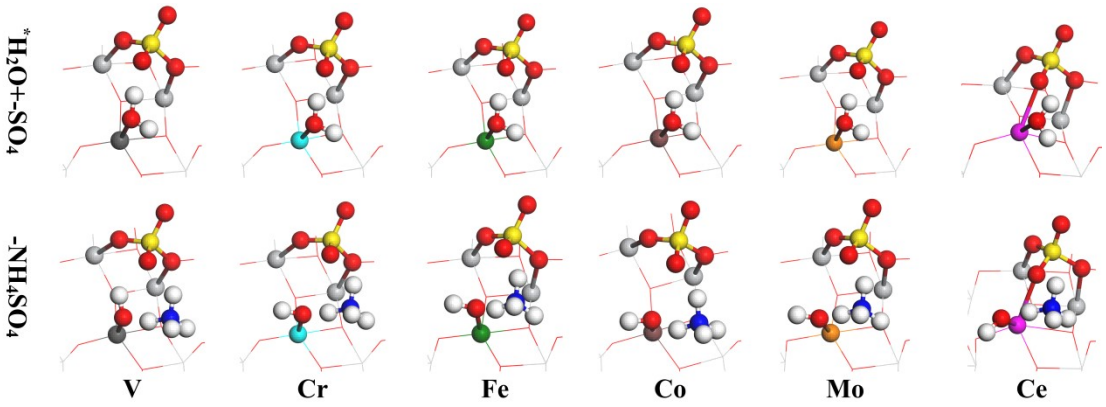

Fig. S4. Configurations of intermediates and products in water-sulfur synergistic poisoning pathways forming -NH_4SO_4 on M-TiO_2 catalysts (M = V, Cr, Fe, Co, Mo, Ce). (Color scheme: dark grey, V; cyan, Cr; green, Fe; brown, Co; orange, Mo; pink, Ce; grey, Ti; red, O; white, H; blue, N; yellow, S)

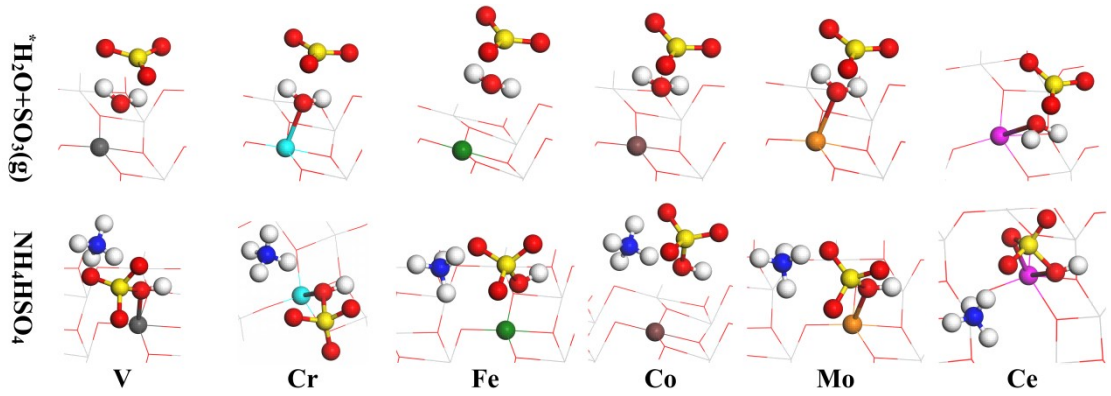

Fig. S5. Configurations of intermediates and products in water-sulfur synergistic poisoning pathways forming NH_4HSO_4 on M-TiO_2 catalysts (M = V, Cr, Fe, Co, Mo, Ce). (Color scheme: dark grey, V; cyan, Cr; green, Fe; brown, Co; orange, Mo; pink, Ce; grey, Ti; red, O; white, H; blue, N; yellow, S)

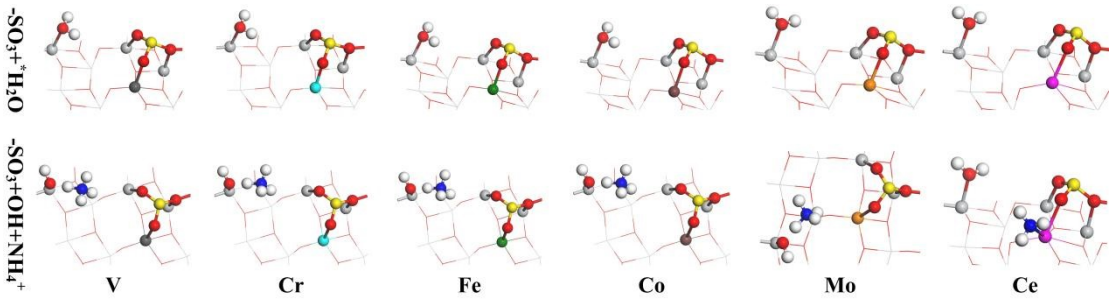

Fig. S6. Configurations of intermediates and products in water-sulfur synergistic poisoning pathways forming -SO_3+OH+NH_4^+ on M-TiO_2 catalysts (M = V, Cr, Fe, Co, Mo, Ce). (Color scheme: dark grey, V; cyan, Cr; green, Fe; brown, Co; orange, Mo; pink, Ce; grey, Ti; red, O; white, H; blue, N; yellow, S)

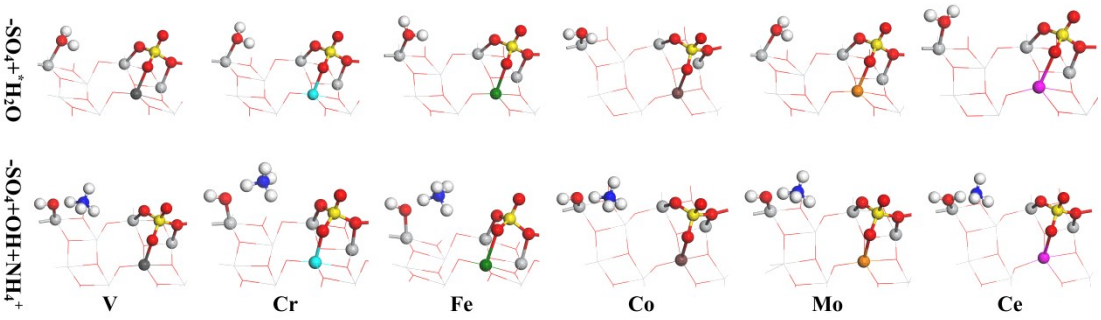

Fig. S7. Configurations of intermediates and products in water-sulfur synergistic poisoning pathways forming $-SO_4+OH+NH_4^+$ on M-TiO_2 catalysts (M = V, Cr, Fe, Co, Mo, Ce). (Color scheme: dark grey, V; cyan, Cr; green, Fe; brown, Co; orange, Mo; pink, Ce; grey, Ti; red, O; white, H; blue, N; yellow, S)

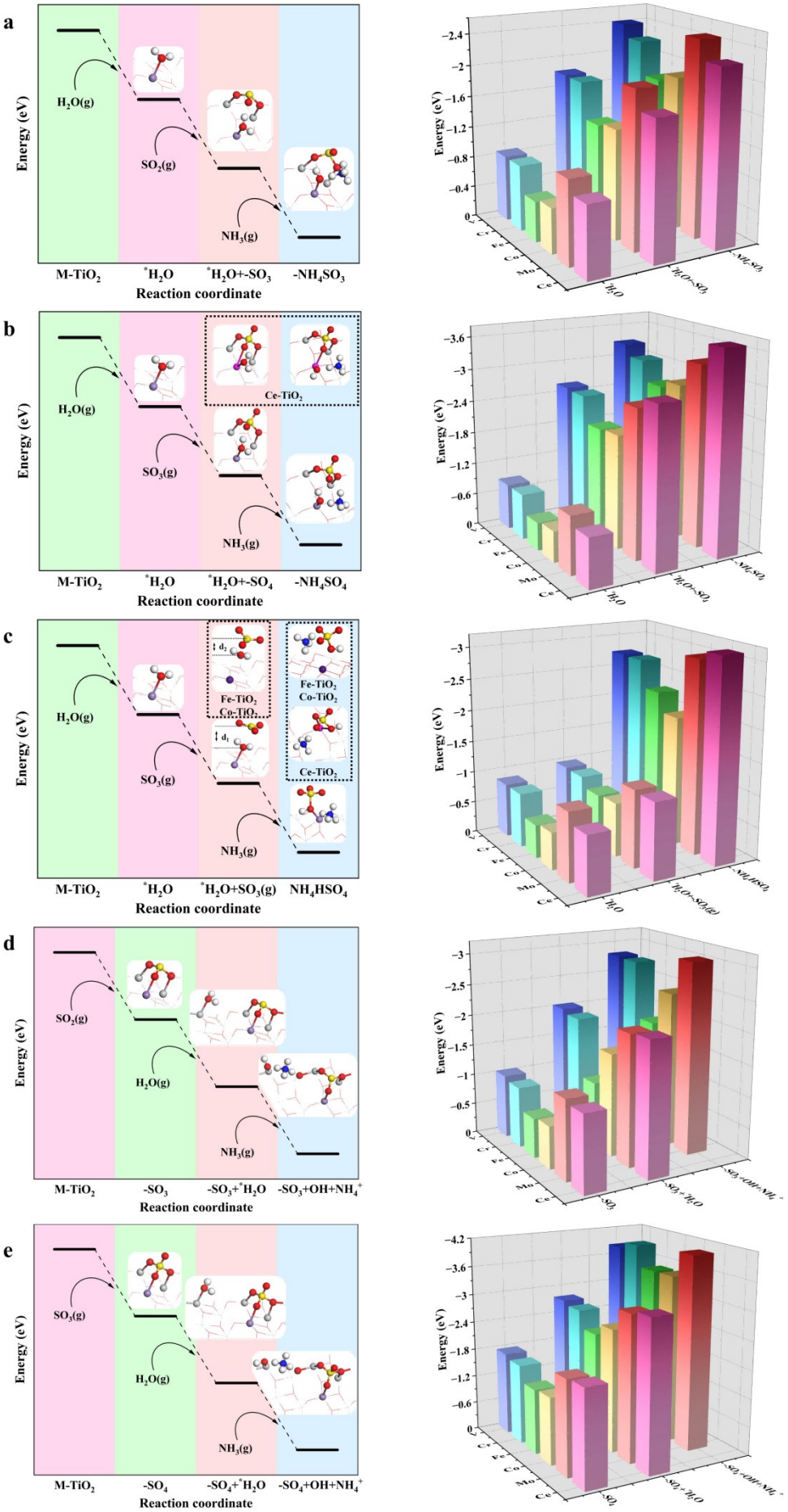
a
Energy (eV)
H2O(g)
SO2(g)
NH3(g)
M-TiO2
*H2O
*H2O+-SO3
-NH4SO3
Reaction coordinate
Energy (eV)
b
Energy (eV)
H2O(g)
SO3(g)
Ce-TiO2
NH3(g)
M-TiO2
*H2O
*H2O+-SO4
-NH4SO4
Reaction coordinate
Energy (eV)
c
Energy (eV)
H2O(g)
SO3(g)
d1
d2
Fe-TiO2
Co-TiO2
Fe-TiO2
Co-TiO2
Ce-TiO2
NH3(g)
M-TiO2
*H2O
*H2O+SO3(g)
NH4HSO4
Reaction coordinate
Energy (eV)
d
Energy (eV)
SO2(g)
H2O(g)
NH3(g)
M-TiO2
-SO3
-SO3+*H2O
-SO3+OH+NH4+
Reaction coordinate
Energy (eV)
e
Energy (eV)
SO3(g)
H2O(g)
NH3(g)
M-TiO2
-SO4
-SO4+*H2O
-SO4+OH+NH4+
Reaction coordinate
Energy (eV)

Fig. S8. Reaction pathways and corresponding energy values of intermediates and products on M-TiO_2 catalysts (M = V, Cr, Fe, Co, Mo, Ce): (a) -NH_4SO_3 formation pathway, (b) -NH_4SO_4 formation pathway, (c) NH_4HSO_4 formation pathway, (d) -SO_3 + H_2O + NH_4^+ formation pathway, (e) -SO_4 + H_2O + NH_4^+ formation pathway. (Color scheme: purple, doped metal M; dark purple, Fe/Co; pink, Ce; grey, Ti; red, O; white, H; blue, N; yellow, S)

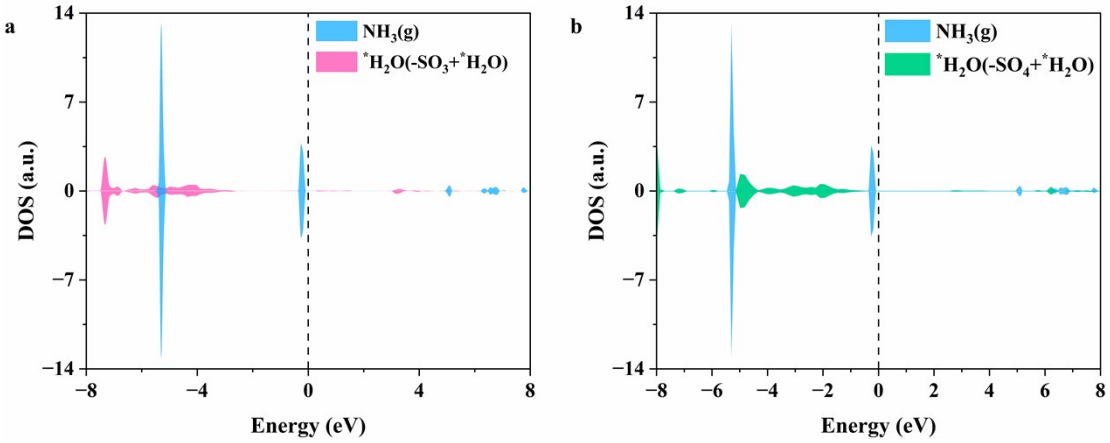

Fig. S9. DOS analysis on Ce-TiO_2 catalyst: (a) $^*H_2O$ in SO_3+$^*H_2O$ with gas-phase NH_3, (b)$^*H_2O$ in SO_4+$^*H_2O$ with gas-phase NH_3.

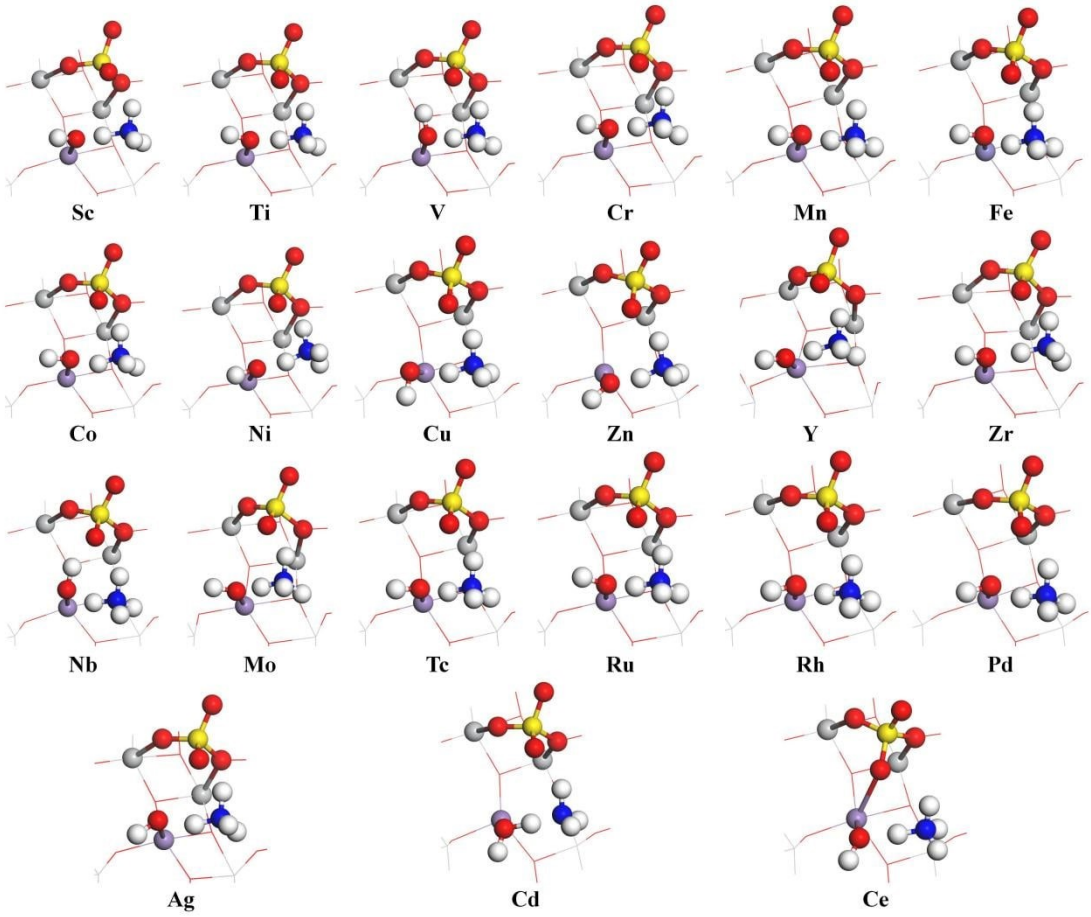

Fig. S10. Configurations of intermediates and products in water-sulfur synergistic poisoning pathways forming -NH_4SO_4 on M-TiO_2 catalysts (M = 3d, 4d transition metals, and Ce). (Color scheme: purple, doped metal M; grey, Ti; red, O; white, H; blue, N; yellow, S)

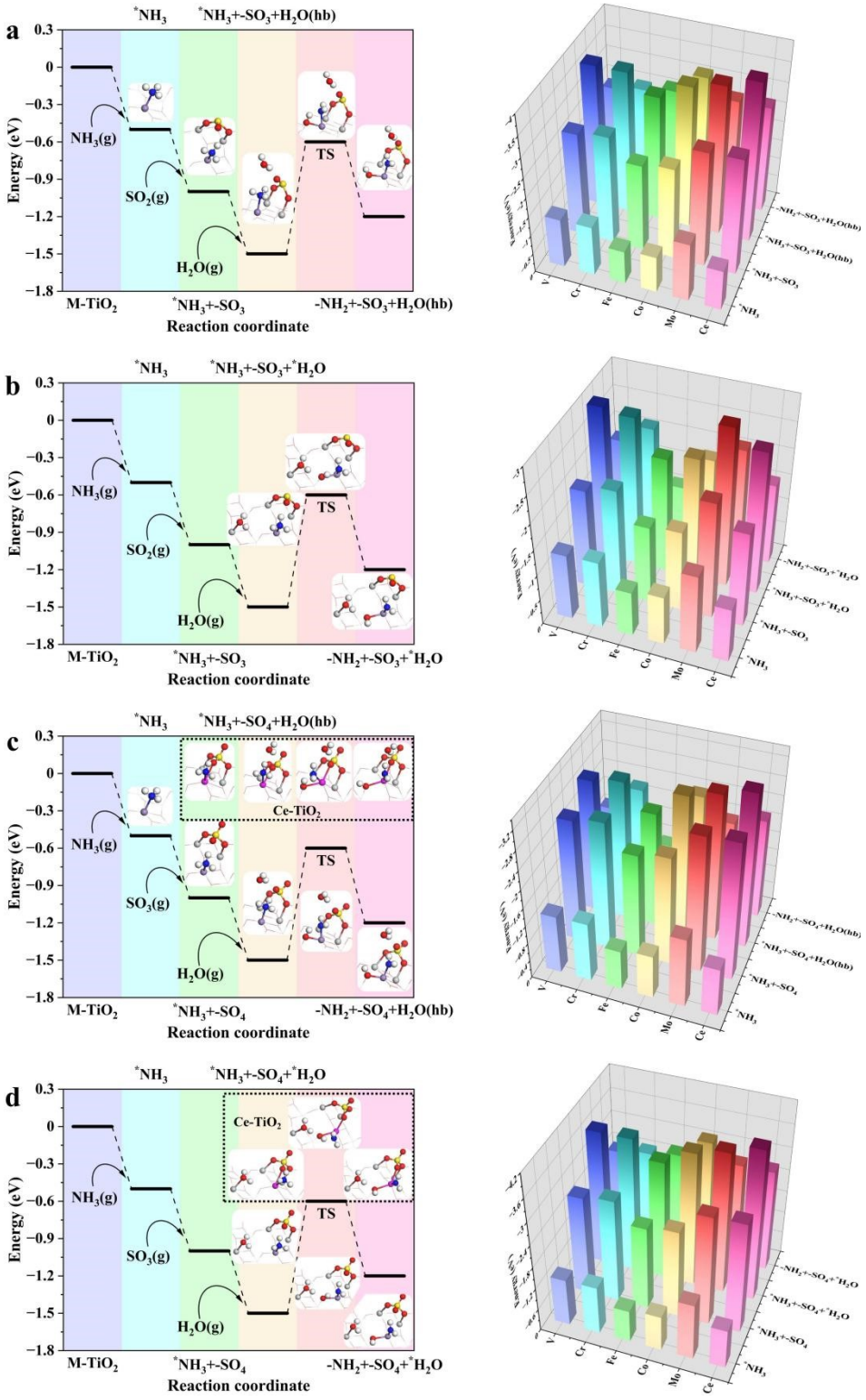

Fig. S11. Reaction pathways and corresponding energy values for NH_3 dissociation to -NH_2 on M-TiO_2 catalysts (M = V, Cr, Fe, Co, Mo, Ce) under four different conditions: (a) -SO_3+H_2O(hb), (b) -SO_3+$^*H_2O$, (c) -SO_4+H_2O(hb), and (d) -SO_4+$^*H_2O$. (Color scheme: purple, doped metal M; pink, Ce; grey, Ti; red, O; white, H; blue, N; yellow, S)

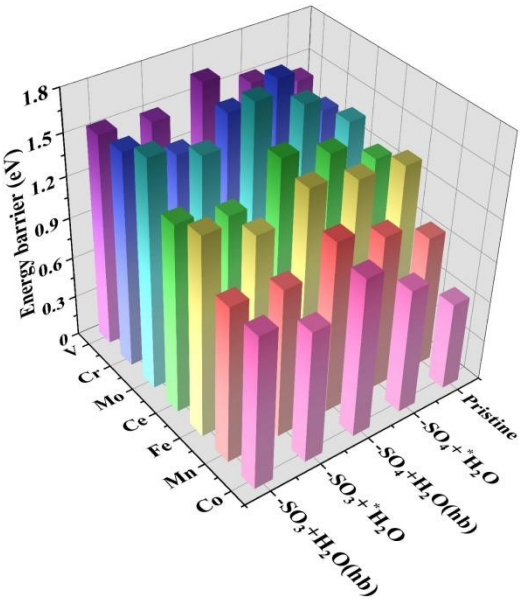

Fig. S12. Energy barriers for NH_3 dissociation to -NH_2 on M-TiO_2 catalysts (M = V, Cr, Fe, Co, Mo, Ce) under four water-sulfur co-existence conditions and on a pristine surface.

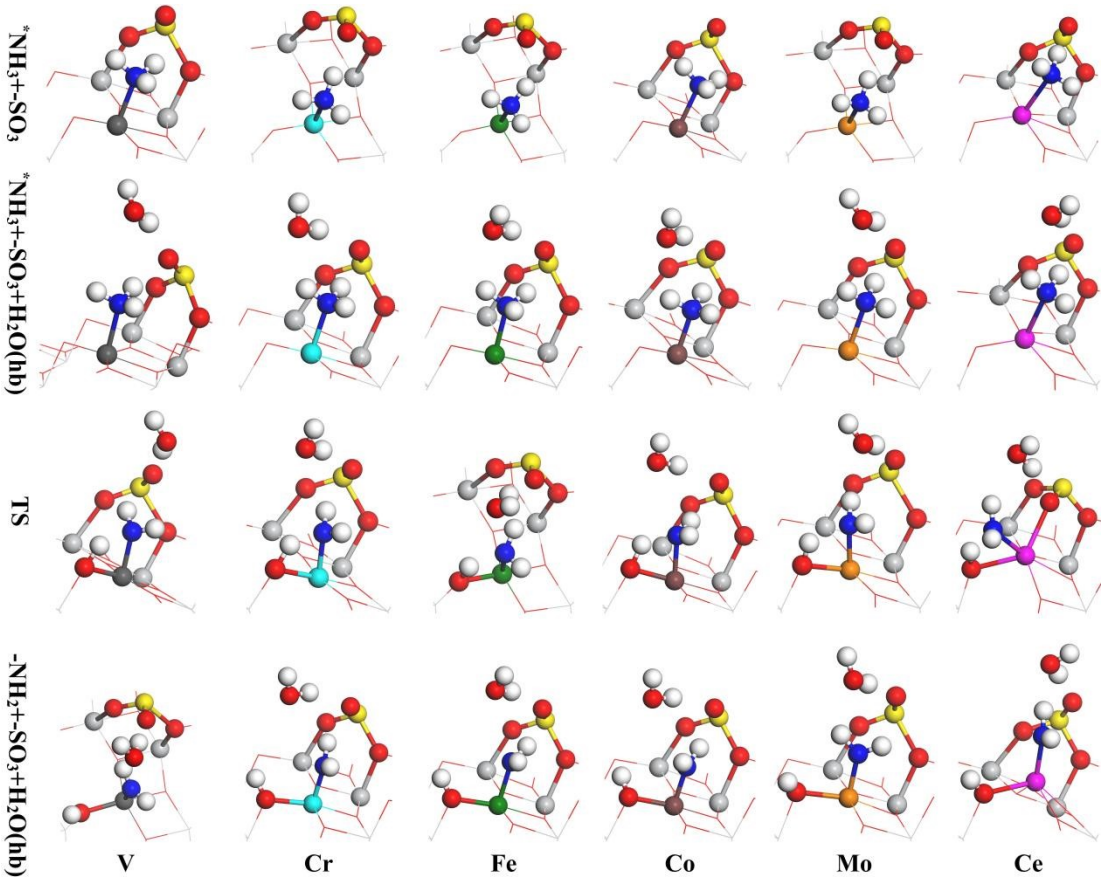

Fig. S13. Configurations of intermediates and products in water-sulfur synergistic poisoning pathways ($-SO_3 + H_2O(hb)$) affecting the NH_3-SCR reaction mechanism on M-TiO_2 catalysts (M = V, Cr, Fe, Co, Mo, Ce). (Color scheme: dark grey, V; cyan, Cr; green, Fe; brown, Co; orange, Mo; pink, Ce; grey, Ti; red, O; white, H; blue, N; yellow, S)

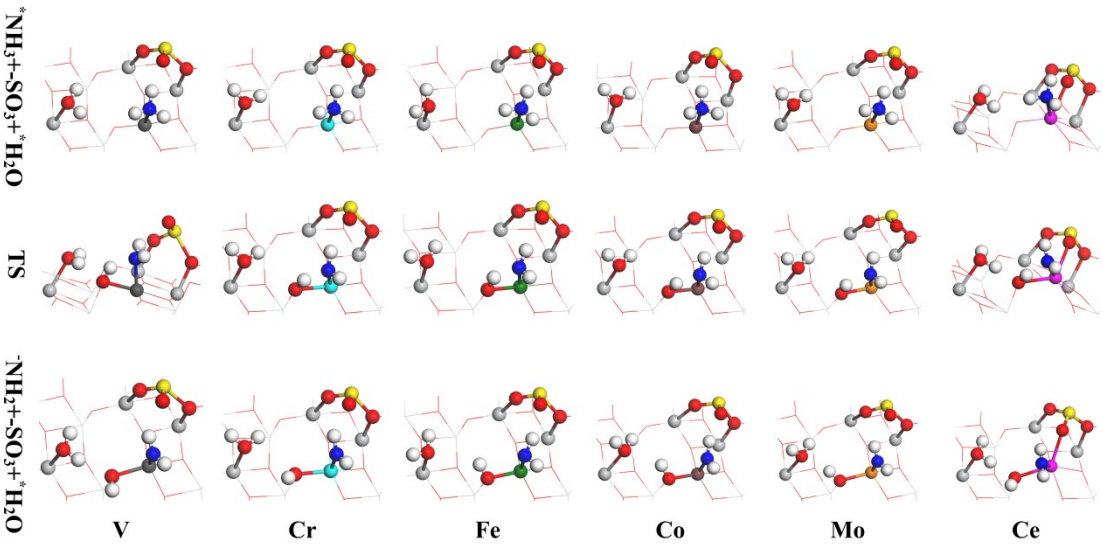

Fig. S14. Configurations of intermediates and products in water-sulfur synergistic poisoning pathways ($-SO_3$ + $^*H_2O$) affecting the NH_3-SCR reaction mechanism on M-TiO_2 catalysts (M = V, Cr, Fe, Co, Mo, Ce). (Color scheme: dark grey, V; cyan, Cr; green, Fe; brown, Co; orange, Mo; pink, Ce; grey, Ti; red, O; white, H; blue, N; yellow, S)

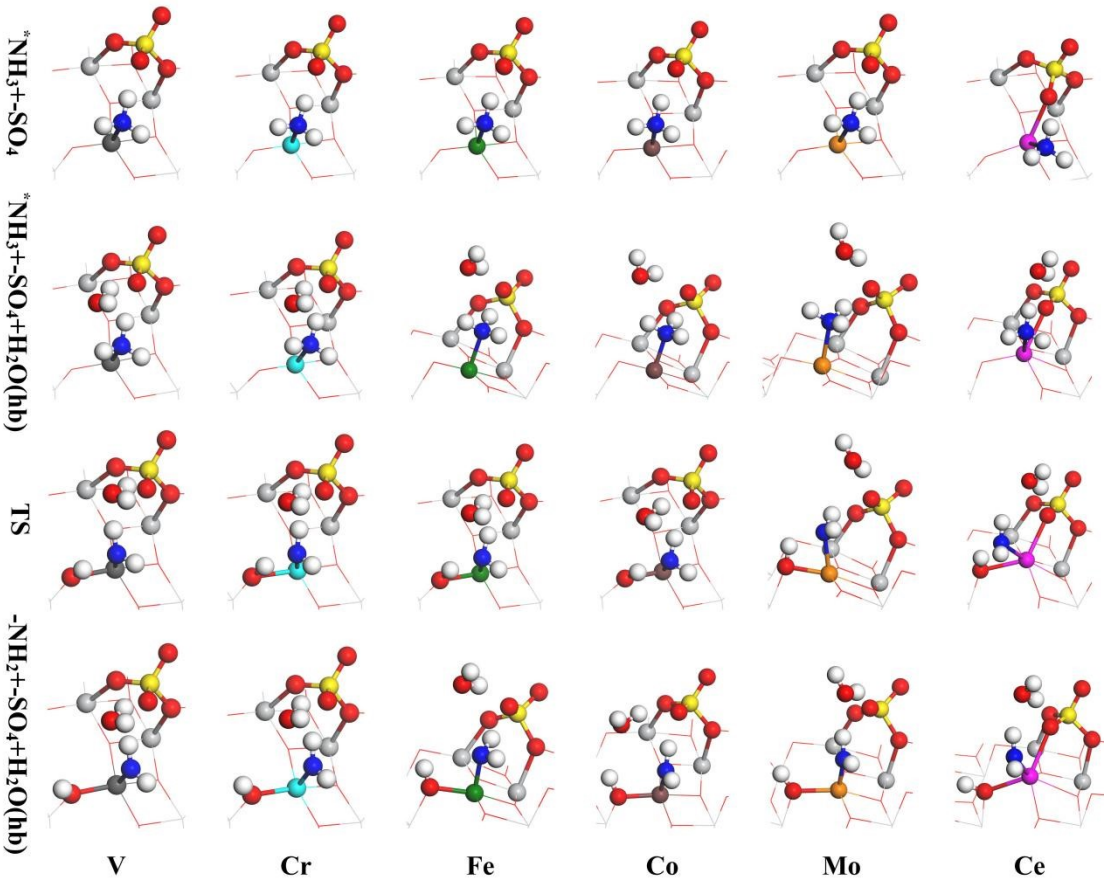

Fig. S15. Configurations of intermediates and products in water-sulfur synergistic poisoning pathways (-SO_4 + H_2O(hb)) affecting the NH_3-SCR reaction mechanism on M-TiO_2 catalysts (M = V, Cr, Fe, Co, Mo, Ce). (Color scheme: dark grey, V; cyan, Cr; green, Fe; brown, Co; orange, Mo; pink, Ce; grey, Ti; red, O; white, H; blue, N; yellow, S)

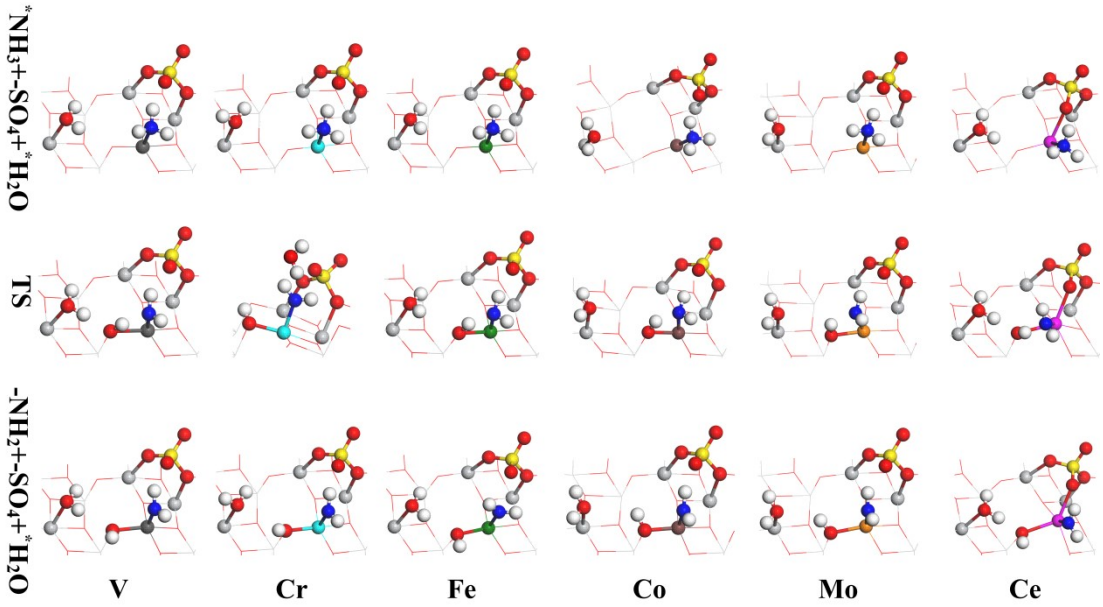

Fig. S16. Configurations of intermediates and products in water-sulfur synergistic poisoning pathways ($-SO_4$ + $^*H_2O$) affecting the NH_3-SCR reaction mechanism on M-TiO_2 catalysts (M = V, Cr, Fe, Co, Mo, Ce). (Color scheme: dark grey, V; cyan, Cr; green, Fe; brown, Co; orange, Mo; pink, Ce; grey, Ti; red, O; white, H; blue, N; yellow, S)

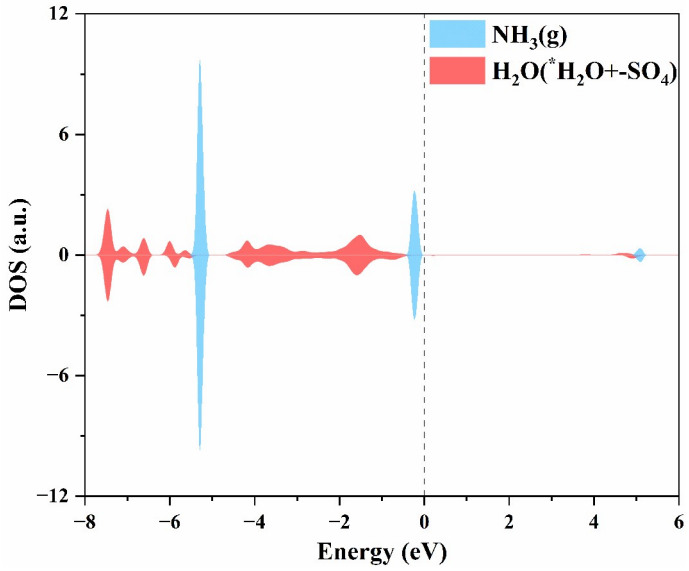

Fig. S17. DOS analysis of H_2O in $^*H_2O$+-SO_4 and gas-phase NH_3 on Cd-TiO_2.

References

[1] G. Kresse, J. Furthmüller. Efficient Iterative Schemes for Ab Initio Total-Energy Calculations Using a Plane-Wave Basis Set[J]. Physical Review. B, Condensed Matter, 1996, 54:11169. https://doi.org/10.1103/PhysRevB.54.11169

[2] G. Kresse; J. Furthmuller. Efficiency of ab-initio total energy calculations for metals and semiconductors using a plane-wave basis set[J]. Computational Materials Science, 1996, 6(1):15-50. https://doi.org/10.1016/0927-0256(96)00008-0

[3] J. P. Perdew, K. Burke, M. Ernzerhof. Generalized gradient approximation made simple[J]. Physical Review Letters, 1996, 77(18): 3865. https://doi.org/10.1103/PhysRevLett.77.3865

[4] P. E. Blöchl. Projector augmented-wave method[J]. Physical review B, 1994, 50(24): 17953. https://doi.org/10.1103/PhysRevB.50.17953

[5] B. J. Morgan, G. W. Watson. A density functional theory +U study of oxygen vacancy formation at the (110),(100),(101), and (001) surfaces of rutile TiO_2[J]. The Journal of Physical Chemistry C, 2009, 113(17): 7322-7328. https://doi.org/10.1021/jp811288n

[6] B. Liu, J. Liu, L. Xin, T. Zhang, Y. Xu, et al. Unraveling Reactivity Descriptors and Structure Sensitivity in Low-Temperature NH_3-SCR Reaction over $CeTiO_x$ Catalysts: A Combined Computational and Experimental Study[J]. ACS Catalysis, 2021, 11(13): 7613-7636. https://doi.org/10.1021/acscatal.1c00311

[7] Z. Zhang, R. Li, M. Wang, Y. Li, Y. Tong, P. Yang, et al. Two steps synthesis of $CeTiO_x$ oxides nanotube catalyst: Enhanced activity, resistance of SO_2 and H_2O for low temperature NH_3-SCR of NO_x[J]. Applied Catalysis B: Environmental, 2021, 282: 119542. https://doi.org/10.1016/j.apcatb.2020.119542

[8] A. Junkaew, M. Ehara, L. Huang, S. Namuangruk. Facet-dependent catalytic activity of anatase TiO_2 for the selective catalytic reduction of NO with NH_3: a dispersion-corrected density functional theory study[J]. Applied Catalysis A: General, 2021, 623: 118250. https://doi.org/10.1016/j.apcata.2021.118250

[9] W. Yin, B. Wen, C. Zhou, A. Selloni, L. Liu. Excess electrons in reduced rutile and anatase TiO_2[J]. Surface Science Reports, 2018, 73(2) : 58-82. https://doi.org/10.1016/j.surfrep.2018.02.003

[10]Q. Li , X. Li, W. Li, L. Zhong, C. Zhang, Q. Fang, et al. Effect of preferential exposure of anatase TiO_2 {0 0 1} facets on the performance of Mn-Ce/TiO_2 catalysts for low-temperature selective catalytic reduction of NO_x with NH_3[J]. Chemical Engineering Journal, 2019, 369: 26-34. https://doi.org/10.1016/j.cej.2019.03.054

[11]Z. Sheng, D. Ma, D. Yu, X. Xiao, B. Huang, L. Yang, et al. Synthesis of novel MnO_x@TiO_2 core-shell nanorod catalyst for low-temperature NH_3-selective catalytic reduction of NO_x with enhanced SO_2 tolerance[J]. Chinese Journal of Catalysis, 2018, 39(4): 821-830. https://doi.org/10.1016/S1872-2067(18)63059-1

[12]A. Junkaew, M. Ehara, L. Huang, S. Namuangruk. Facet-dependent catalytic activity of anatase TiO_2 for the selective catalytic reduction of NO with NH_3: a dispersion-corrected density functional theory study[J]. Applied Catalysis A: General, 2021, 623: 118250. https://doi.org/10.1016/j.apcata.2021.118250

[13]W. Yin, B. Wen, C. Zhou, A. Selloni, L. Liu. Excess electrons in reduced rutile and anatase TiO_2[J]. Surface Science Reports, 2018, 73(2) : 58-82. https://doi.org/10.1016/j.surfrep.2018.02.003

[14]Q. Li , X. Li, W. Li, L. Zhong, C. Zhang, et al. Effect of preferential exposure of anatase TiO_2 {0 0 1} facets on the performance of Mn-Ce/TiO_2 catalysts for low-temperature selective catalytic reduction of NO_x with NH_3[J]. Chemical Engineering Journal, 2019, 369: 26-34. https://doi.org/10.1016/j.cej.2019.03.054

[15]Z. Sheng, D. Ma, D. Yu, X. Xiao, B. Huang, et al. Synthesis of novel MnO_x@TiO_2 core-shell nanorod catalyst for low-temperature NH_3-selective catalytic reduction of NO_x with enhanced SO_2 tolerance[J]. Chinese Journal of Catalysis, 2018, 39(4): 821-830. https://doi.org/10.1016/S1872-2067(18)63059-1

[16]T. Weirich, M. Winterer, S. Seifried, H. Hahn, H. Fuess. Rietveld analysis of electron powder diffraction data from nanocrystalline anatase, TiO_2[J]. Ultramicroscopy, 2000, 81(3-4): 263-270. https://doi.org/10.1016/S0304-3991(99)00189-8

[17]H. Zheng, W. Song, Y. Zhou, S. Ma, J. Deng, Y. Li, et al. Mechanistic Study of Selective Catalytic Reduction of NO_x with NH_3 over Mn-TiO_2: A Combination of Experimental and DFT Study[J]. The Journal of Physical Chemistry C, 2017, 121(36): 19859-19871. https://doi.org/10.1021/acs.jpcc.7b06715

[18]H. Zheng, R. Li, C. Zhong, Z. Li, Y. Kang, J. Deng, et al. Theoretical design of transition metal-doped TiO_2 for the selective catalytic reduction of NO with NH_3 by DFT calculations[J]. Catalysis Science & Technology, 2022, 12(5): 1429-1440. https://doi.org/10.1039/D1CY02214H

[19]G. Henkelman, B. Uberuaga, H. Jonsson. A climbing image nudged elastic band method for finding saddle points and minimum energy paths[J]. The Journal of Chemical Physics, 2000, 113(22): 9901-9904. https://doi.org/10.1063/1.1329672

[20]Q. Meng, T. Wang, E. Liu, X. Ma, Q. Geac, J. Gong. Understanding electronic and optical properties of anatase TiO_2 photocatalysts co-doped with nitrogen and transition metals[J]. Physical Chemistry Chemical Physics, 2013, 15(24): 9549-9561. https://doi.org/10.1039/C3CP51476E

[21]F. Liu, H. He, Y. Ding, C. Zhang. Effect of manganese substitution on the structure and activity of iron titanate catalyst for the selective catalytic reduction of NO with NH_3[J]. Applied Catalysis B: Environmental, 2009, 93(1-2): 194-204. https://doi.org/10.1016/j.apcatb.2009.09.029

[22]L. Jesus, G. Horrocks, Y. Liang, A. Parija, C. Jaye, L. Wangoh, et al. Mapping polaronic states and lithiation gradients in individual V_2O_5 nanowires[J]. Nature Communications, 2016, 7(1): 1-9. https://doi.org/10.1038/ncomms12022

[23]A. Jain, G. Hautier, S. Ong, C. J. Moore, C. C. Fischer, K. A. Persson, et al. Formation enthalpies by mixing GGA and GGA+U calculations[J]. Physical Review B, 2011, 84(4): 045115. https://doi.org/10.1103/PhysRevB.84.045115

[24]O. D Alessandro, D. Pintos, A. Juan, B. Irigoyen, J. Sambeth. A DFT study of phenol adsorption on a low doping Mn-Ce composite oxide model[J]. Applied Surface Science, 2015, 359: 14-20. https://doi.org/10.1016/j.apsusc.2015.09.266

[25]B. Himmetoglu, R. Wentzcovitch, M. Cococcioni. First-principles study of electronic and structural properties of CuO[J]. Physical Review B, 2011, 84(11): 115108. https://doi.org/10.1103/PhysRevB.84.115108

[26]L. Bendavid, E. Carter. CO_2 adsorption on $Cu_2O(111)$: a DFT+U and DFT-D study[J]. The Journal of Physical Chemistry C, 2013, 117(49): 26048-26059.

https://doi.org/10.1021/jp407468t

[27]S. Haffad, K. Kiprono. Interfacial structure and electronic properties of TiO_2/ZnO/TiO_2 for photocatalytic and photovoltaic applications: a theoretical study[J]. Surface Science, 2019, 686: 10-16. https://doi.org/10.1016/j.susc.2019.03.006

[28]B. Saha, T. Sands, U. Waghmare. Electronic structure, vibrational spectrum, and thermal properties of yttrium nitride: a first-principles study[J]. Journal of Applied Physics, 2011, 109(7): 073720. https://doi.org/10.1063/1.3561499

[29]Y. Tang, S. Zhao, B. Long , J. Liu, J. Li. On the nature of support effects of metal dioxides MO_2 (M=Ti, Zr, Hf, Ce, Th) in single-atom gold catalysts: importance of quantum primogenic effect[J]. The Journal of Physical Chemistry C, 2016, 120(31): 17514-17526. https://doi.org/10.1021/acs.jpcc.6b05338

[30]D. Ren, H. Li, X. Cheng. Tailoring the electronic and optical properties of anatase TiO_2 by (S, Nb) co-doping from a DFT plus U calculation[J]. Solid State Communications, 2015, 223: 54-59. https://doi.org/10.1016/j.ssc.2015.09.011

[31]L. Bai, B. Zheng, J. Lian, Q. Jiang. First-principles calculations of Cd-doped ZnO thin films deposited by pulse laser deposition[J]. Solid State Sciences, 2012, 14(6): 698-704. https://doi.org/10.1016/j.solidstatesciences.2012.03.018

[32]W. Song, J.Liu, H. Zheng, S. Ma, Y. Wei, A. Duan, et al. A mechanistic DFT study of low temperature SCR of NO with NH_3 on $MnCe_{1-x}O_2$(111)[J]. Catalysis Science & Technology, 2016, 6(7): 2120-2128. https://doi.org/10.1039/C5CY01597A